LPV modeling of a flexible wing aircraft using modal alignment and adaptive gridding methods

Ali Khudhair Al-Jiboory [a,b], Guoming Zhu [a,*], Sean Shan-Min Swei [c], Weihua Su [d], Nhan T. Nguyen [c]

[a] *Mechanical Engineering, Michigan State University, East Lansing, MI 48823, United States*
[b] *College of Engineering, University of Diyala, Baqubah, Iraq*
[c] *Intelligent Systems Division, NASA Ames Research Center, United States*
[d] *Department of Aerospace Engineering and Mechanics, University of Alabama, Tuscaloosa, AL, United States*

ABSTRACT

One of the earliest approaches in gain-scheduling control is the *gridding* based approach, in which a set of local linear time-invariant models are obtained at various gridded points corresponding to the varying parameters within the flight envelop. In order to ensure smooth and effective Linear Parameter-Varying control, aligning all the flexible modes within each local model and maintaining small number of representative local models over the gridded parameter space are crucial. In addition, since the flexible structural models tend to have large dimensions, a tractable model reduction process is necessary. In this paper, the notion of σ-shifted $\mathscr{H}_2$- and $\mathscr{H}_\infty$-norm are introduced and used as a metric to measure the model mismatch. A new modal alignment algorithm is developed which utilizes the defined metric for aligning all the local models over the entire gridded parameter space. Furthermore, an Adaptive Grid Step Size Determination algorithm is developed to minimize the number of local models required to represent the gridded parameter space. For model reduction, we propose to utilize the concept of Composite Modal Cost Analysis, through which the collective contribution of each flexible mode is computed and ranked. Therefore, a reduced-order model is constructed by retaining only those modes with significant contribution. The NASA Generic Transport Model operating at various flight speeds is studied for verification purpose, and the analysis and simulation results demonstrate the effectiveness of the proposed modeling approach.

© 2017 Elsevier Masson SAS. All rights reserved.

1. Introduction

At the advent of advanced composite materials technology, lightweight aircraft design concept has attracted considerable attentions in recent years in an effort to improve the aerodynamic efficiency. However, as the flexibility of a structure increases, aeroelastic interactions with aircraft aerodynamic forces and moments can have adverse impact on aircraft's stability and performance. Therefore, active control of aeroelastic aircraft is becoming increasingly important, especially for aircraft with highly flexible wings. The objectives of flight control design are to guarantee the closed-loop stability and to improve the handling qualities over a wide range of flight conditions. Generally, these objectives cannot be achieved using just one single flight controller operating over the entire flight envelop, due to the notable variations on rigid body aerodynamics and aeroelasticity within the flight profile.

One effective remedy for this challenging problem is to directly synthesize Linear Parameter-Varying (LPV) controller [1] for the entire flight envelop [2–5]. This approach has been demonstrated to be very promising for various aerospace applications [6–9]. Although many theoretical results were developed and applied to the special class of nonlinear and/or parameter-varying systems, the essential requirement for these theories to work is to have a representative LPV model that captures the varying nature of the system dynamics. In general, there are two ways to attain the needed LPV model. If a mathematical model is difficult to attain [10], a global [11] or local [12] system identification technique can be applied to identify the LPV model. In the global system identification approach, a single experiment has to be performed such that all scheduling parameters are excited simultaneously and persistently [13], which is not always possible in practice. On the other hand, local system identification approach requires performing multiple experiments with fixed scheduling parameters [14] at various op-

* Corresponding author.
E-mail address: zhug@egr.msu.edu (G. Zhu).

erating points, leading to a set of local linear time-invariant (LTI) models that need to be interpolated to obtain the LPV model. However, the main drawback associated with local methods is the lack of information for the rate of change of scheduling parameter since these LTI models are obtained by freezing scheduling parameters at predefined points.

In the context of attaining aeroelastic models suitable for robust and LPV control, a number of research has been conducted recently, see for instance [15–18]. Some of these studies assume the availability of the analytical models [19–21], which is not practical since most of the large scale aerospace structures are obtained via finite element analysis method, hence they are discrete in nature. In Varga et al. [22] and Puyou and Losser [23], high-fidelity models were considered that included both rigid and flexible dynamics of a civilian aircraft. However, direct interpolation is not possible due to the inconsistency of their state-space representations at different operating points. Similar results were reported in Ferreres [10] and Roos [24], where empirical criteria and physical knowledge of the system were required to obtain the LPV model. Recently, the problem of modal matching and model reduction were considered in Theis et al. [15]. A set of criteria were introduced for modal alignment, based on the modal frequency, damping ratio, and the "B" and "C" matrices associated with each mode. For model reduction, truncation, residualization, and balanced coordinate transformation approaches were utilized to reduce system order sequentially, and the ν-gap metric was used to measure the distance between the reduced-order models (ROMs) and full-order models (FOMs). These approaches were applied to study the Body Freedom Flutter (BFF) air vehicle. Similar approach was used in [25] for BFF aircraft structure. In [16], a procedure was developed to derive reduced-order LPV model from a given set of large-scale LTI models at grid points. $\mathcal{H}_2$-norm was used to measure the distance between FOMs and ROMs. However, the approach was formulated in the Linear Fractional Representation (LFR) framework. The tensor product model transformation technique was proposed in Baranyi and Takarics [17,18], in which the LPV state-space models were transformed into parameter varying convex combination of LTI models through high-order singular value decomposition process. As a result, only those LTI models representing polytopic vertices were needed for subsequent control design. Although modeling and control of aeroelastic aircraft in LPV framework have been studied extensively in the literature, the topic still remains as a challenging research subject and needs to be explored.

The main contributions of this paper are as follows. First, we reexamine the linear interpolation approach. It is found that when interpolating two aeroelastic LTI models operating at two different flight conditions, the resultant interpolated model can be erroneous, especially when performed in modal coordinates. This is because the sequential order of the flexible modes at two different operating conditions might be different, hence resulting in a model mismatch when interpolating the two models. Therefore, a special care must be taken to ensure that the flexible modes are consistently ordered throughout operating conditions before performing interpolation between any two LTI models. For this purpose, a novel Modal Alignment Algorithm (MAA) is developed to align all aeroelastic modes for a given set of LTI models sampled over the flight envelop, so that all LTI models have consistent modal sequence. Second, the number of LTI models needed to approximate the aerodynamic variations within the flight envelop can be minimized. With the current advanced computational power and software technologies, it is not difficult to generate a large number of LTI models with very fine grid points that cover the entire flight envelop. While this large number of LTI models helps improve modeling accuracy, it unnecessarily burdens the flight control design and implementation efforts, since a flight controller must be designed for each local LTI model. Particularly, in the framework of switched LPV controls, it is always desirable to work with a small number of LTI models for control design. This will keep the number of controller switching minimal, while avoiding high order dependency on scheduling parameters. In this paper, we propose an Adaptive Grid Step Size Determination (AGSSD) algorithm, through which a trade-off between the number of local LTI models and the modeling accuracy with guaranteed error bound can be assessed. Finally, each LTI model might contain large number of aeroelastic modes; in addition to the rigid body dynamics, which makes the control design impractical. A novel model reduction process called Composite Modal Cost Analysis (CMCA) is developed to attain a reduced-order model which is better suited for the control design. The essence of CMCA is to utilize the collective contribution of each aeroelastic mode throughout the gridded parameter space and retain those modes with significant contribution.

The approach presented above consists of the following four steps. First, the modal coordinate transformation is utilized to convert the original LTI models into the modal canonical forms, where each modal representation is decoupled. Second, a modified $\mathcal{H}_2$-norm is used to compute the alignment error between each mode and the modes of neighboring LTI models. To better handle the situation where a LTI model has unstable modes, a σ-shifted $\mathcal{H}_2$-norm, denoted by $\mathcal{H}_{(\sigma-2)}$-norm, is defined by shifting the imaginary axis of the complex plane to the right by σ amount, where $\sigma > 0$ is chosen to be sufficiently large so that the $\mathcal{H}_{(\sigma-2)}$-norm of a transfer function is well defined. The $\mathcal{H}_{(\sigma-2)}$-norm of the error transfer function between modes of adjacent LTI models is used as the modal matching criteria. This criteria proves to be effective and plays a crucial role in determining the level of alignment, in that the smallest value indicates the closest of the two modes and hence should be assigned to the same index order throughout the LTI models over the gridded parameter space. Similarly, a σ-shifted $\mathcal{H}_\infty$-norm, denoted by $\mathcal{H}_{(\sigma-\infty)}$-norm, is defined as another modal matching criteria. Third, for a given $\mathcal{H}_{(\sigma-2)}$-norm or $\mathcal{H}_{(\sigma-\infty)}$-norm error bound, an AGSSD algorithm is developed to minimize the number of LTI models needed for linear interpolations over the gridded parameter space. This algorithm proves to be effective and can significantly reduce the required number of LTI models, while providing a balanced trade-off with model accuracy. This result is especially critical for LPV-based control design. Finally, a CMCA method is used to obtain a set of reduced-order LTI models for actual flight controller design. In summary, the proposed approach not only reduces the total number of LTI models needed for covering the entire flight envelop, but also reduces the order of each LTI model so that designing an effective flight controller becomes more tractable.

For ease of presentation, we make use of the NASA Generic Transport Model (GTM) in longitudinal direction operating at various flight speeds to illustrate the proposed LPV modeling approach described above. In particular, the GTM under consideration consists of a short period mode and 20 aeroelastic modes, and its flight speed ranges from Mach 0.5 to Mach 0.88 at a constant cruising altitude. It should be noted that at Mach 0.78, the aeroelastic wing is already exhibiting fluttering behavior, since in this condition the first torsional mode becomes unstable. Both time-domain and frequency-domain simulations will be used to demonstrate the effectiveness of the proposed modeling concept.

The rest of the paper is organized as follows. Section 2 presents mode alignment procedure that consists of modal coordinate transformation and alignment algorithm. A novel AGSSD algorithm is developed in Section 3 to minimize the number of local LTI models over the parameter space. A model reduction process using CMCA is presented in Section 4, which is used to extract a reduced-order model set containing the dominant aeroelastic modes. Some concluding remarks are given in Section 5.

2. Modal alignment for multiple aeroelastic models

This section presents a novel procedure to align aeroelastic modes of multi-input multi-output (MIMO) LTI models generated from various operating conditions within the flight envelop. This procedure guarantees the consistency of the modal representation for LTI models, which can then be used for LPV controller design.

2.1. Modal coordinate transformation

Consider the following collection of LTI dynamical systems,

$$\mathbf{G}^i : \begin{cases} \dot{x}(t) = \mathbf{A}^i x(t) + \mathbf{B}^i u(t) \\ y(t) = \mathbf{C}^i x(t) \end{cases} \quad i = 1, 2, \cdots, p, \quad (1)$$

where $\mathbf{G}^i$ represents the aeroelastic LTI model at operating point i, in which $x(t) \in \mathbb{R}^{n_x}$ denotes the state, $u(t) \in \mathbb{R}^{n_u}$ the input, and $y(t) \in \mathbb{R}^{n_y}$ the output. We assume there are p gridded points in the parameter space within the flight envelop, which also corresponds to the number of local LTI models. Furthermore, we assume that each LTI model contains m flexible modes. Performing modal coordinate transformation [26] to each local LTI model $\mathbf{G}^i$ described in (1) yields

$$\mathscr{G}^i : \begin{cases} \dot{x}(t) = \mathscr{A}^i x(t) + \mathscr{B}^i u(t) \\ y(t) = \mathscr{C}^i x(t) \end{cases} \quad i = 1, 2, \cdots, p, \quad (2)$$

where the system matrices are partitioned as follows,

$$\mathscr{A}^i = \begin{bmatrix} A_1^i & \mathbf{0} & \cdots & \mathbf{0} \\ \mathbf{0} & A_2^i & \ddots & \vdots \\ \vdots & \ddots & \ddots & \mathbf{0} \\ \mathbf{0} & \cdots & \mathbf{0} & A_m^i \end{bmatrix}; \quad A_j^i = \begin{bmatrix} a_j^i & b_j^i \\ -b_j^i & a_j^i \end{bmatrix},$$

$$\mathscr{B}^i = \begin{bmatrix} B_1^i \\ B_2^i \\ \vdots \\ B_m^i \end{bmatrix}, \quad \mathscr{C}^i = \begin{bmatrix} C_1^i & C_2^i & \cdots & C_m^i \end{bmatrix}. \quad (3)$$

Note that A_j^i denotes a real matrix form for a pair of complex eigenvalues $\lambda_j^i = a_j^i \pm jb_j^i$, where λ_j^i denotes the jth eigenvalue of the ith LTI model, hence each A_j^i represents a flexible mode. In this study, we consider two sources of modal mismatch when aligning modes from two different aeroelastic LTI models. In general, the sequential order of modal frequencies and mode shapes between the two LTI models $\mathscr{G}^i$ and $\mathscr{G}^k$, where $k \in [1, 2, \cdots, p]$ and $k \neq i$. That is, the sequential order of block diagonal elements in $\mathscr{A}^i$ and $\mathscr{A}^k$ might not be aligned, and this misalignment is caused by the notable variations in aeroelastic behaviors from one flight condition to another, such that the order of one or more modes is reversed when comparing the two LTI models; see for instance Fig. 1(a). As a consequence, performing linear interpolation between $\mathscr{G}^i$ and $\mathscr{G}^k$ will result in an erroneous, mismatched LTI model. Another source of modal mismatch is the variations in the plant matrices $\mathscr{B}^i$ and $\mathscr{C}^i$ that could lead to different normalization with respect to each mode [15].

Since the aeroelastic dynamics vary continuously over the varying parameters, we adopt the transfer function representation to describe the modal dynamics for each given LTI model.

2.2. Modal alignment algorithm

From the structure of $\mathscr{G}^i$ described in (2) and (3), the modal transfer function for each mode in $\mathscr{G}^i$ can be expressed as
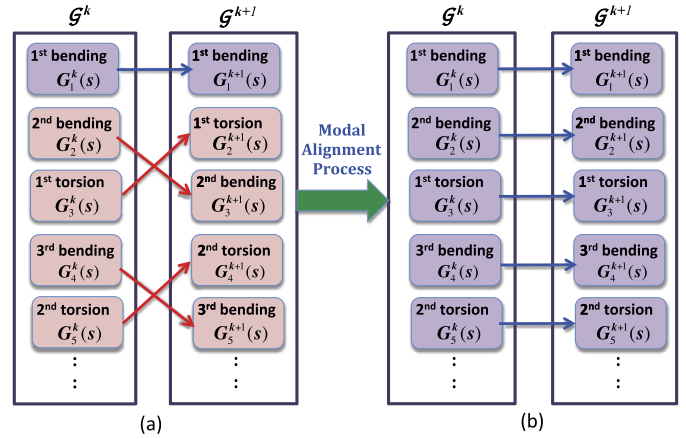

Fig. 1. An illustration of modal alignment process (a) misaligned modes (b) aligned modes.

$$G_j^i(s) = C_j^i(sI - A_j^i)^{-1}B_j^i, \quad j = 1, 2, \cdots, m; \ i = 1, 2, \cdots, p, \quad (4)$$

and the total transfer function for each LTI model $\mathscr{G}^i$ in (2) can be written as a sum of individual modal transfer function as follows,

$$\mathscr{G}^i(s) := \sum_{j=1}^m G_j^i(s) = \sum_{j=1}^m C_j^i(sI - A_j^i)^{-1}B_j^i, \quad i = 1, 2, \cdots, p. \quad (5)$$

The goal of this section is to develop an automated alignment method to match modes with the closest dynamic properties at neighboring LTI models, such that all local LTI models will have consistent realizations suitable for LPV control design. To this end, we assume that all the local systems are already transformed into the modal transfer function form as given in (4). The modal alignment objective is to identify the closest match of the jth mode at ith grid point $G_j^i(s)$ with the kth modes $G_k^{i+1}(s)$ at the neighboring $(i+1)$th grid point, where $j, k = 1, \cdots, m$. Therefore, once a matched mode is identified, the sequential order of modes in $\mathscr{G}^{i+1}$ needs to be permuted so that the jth mode at $(i+1)$th grid point has the same order (index) as the jth mode at ith grid point. Fig. 1(b) shows the aligned aeroelastic modes within each LTI model. This framework will be used in Section 3 for developing AGSSD algorithm.

A modified $\mathscr{H}_2$-norm is proposed as a means to measure the modal mismatch. Note that the $\mathscr{H}_2$-norm for a stable jth mode at ith grid point $G_j^i(s)$ is defined as [27]

$$\|G_j^i(s)\|_2^2 = \text{trace}(C_j^i P_j^i C_j^{i'}),$$

where $P_j^i > 0$ is the unique solution to the following Lyapunov matrix equation,

$$A_j^i P_j^i + P_j^i A_j^{i'} + B_j^i B_j^{i'} = 0. \quad (6)$$

Note that the $\mathscr{H}_2$-norm is only defined for the stable systems, however, for a flexible wing aircraft, some aeroelastic modes can become unstable or flutter at higher Mach number, in which case the $\mathscr{H}_2$-norm is not defined. To handle this situation, we introduce a notion of relative stability in frequency domain by shifting the imaginary axis to the right by σ amount, such that in the new shifted complex plane, all modes become stable hence we can compute the $\mathscr{H}_2$ norm for each modal error transfer function. Mathematically, this frequency shift concept can be described as follows,

$$G_j^i(s + \sigma) = C_j^i[(s + \sigma)I - A_j^i]^{-1}B_j^i, \quad j = 1, 2, \cdots, m; \ i = 1, 2, \cdots, p, \quad (7)$$

where $\sigma > 0$ is properly chosen such that it is greater than the largest positive real part of all unstable modes over the LTI model set. Therefore, the notion of $\mathscr{H}_{(\sigma-2)}$-norm is defined as follows,

$$\|G_j^i(s)\|_{\sigma-2}^2 = \|G_j^i(s+\sigma)\|_2^2 = \text{trace}(C_j^i \bar{P}_j^i C_j^{i'}), \tag{8}$$

where $\bar{P}_j^i > 0$ satisfies the following Lyapunov equation,

$$(A_j^i - \sigma I)\bar{P}_j^i + \bar{P}_j^i(A_j^i - \sigma I)' + B_j^i B_j^{i'} = 0. \tag{9}$$

As mentioned earlier, by shifting the imaginary axis to the right by σ, the resulting system matrix $A_j^i - \sigma I$ will be stable so that the $\mathscr{H}_{(\sigma-2)}$-norm is well-defined. Similarly, we can introduce the $\mathscr{H}_{(\sigma-\infty)}$-norm of a rational transfer function as

$$\|G_j^i(s)\|_{\sigma-\infty} = \|G_j^i(s+\sigma)\|_\infty, \tag{10}$$

in which the $\mathscr{H}_\infty$-norm is defined as

$$\|G_j^i(s)\|_\infty = \sup_\omega \{\sigma_{max}(G_j^i(j\omega))\}, \tag{11}$$

where $\sigma_{\max}(\cdot)$ denotes the maximum singular value.

After transforming all the transfer functions into the shifted frequency domain, the following $\mathscr{H}_{(\sigma-2)}$ criterion is used to measure the *distance* between any two modes of the two neighboring grid points, i and $i+1$,

$$M_j^{i+1} = \|G_j^i(s) - G_k^{i+1}(s)\|_{\sigma-2}, \\ i = 1, 2, \cdots, p-1, \quad j, k = 1, 2, \cdots, m, \tag{12}$$

where M_j^{i+1} denotes the $\mathscr{H}_{(\sigma-2)}$-norm of the error transfer function between the jth mode at grid point i and the kth mode at grid point $i+1$. Note that the smallest value will indicate the two modes have the similar dynamic properties. By utilizing (12) for all j and k, we can identify the correct permutation index in $\mathscr{G}^{i+1}$ so that all modes in $\mathscr{G}^i$ and $\mathscr{G}^{i+1}$ are sequentially aligned. Thus, this alignment process guarantees consistent variations of the flexible modes over the entire flight envelope. Algorithm 1 in Fig. 2 illustrates this iterative modal alignment process.

As mentioned earlier, the proposed approach is applied to the NASA Generic Transport Model (GTM) shown in Fig. 3. A set of 18 local LTI models are generated according to various flight speeds ranging from Mach 0.5 to Mach 0.88, as shown in Table 1. We assume that both longitudinal rigid body states and aeroelastic wing states are available for measurement. For aeroelastic measurement, as depicted in Fig. 3, we take outputs from 5 equally spaced data points for both bending and torsional displacements and their rates. Each local LTI model consists of 20 aeroelastic modes and one rigid body short period mode. However, in this study, we focus only on the aeroelastic modes, hence we set $p = 18$ and $m = 20$.

To demonstrate the effectiveness of the proposed modal alignment process, the modes within each LTI model are intentionally shuffled to generate modal inconsistency among LTI models. Fig. 4 illustrates before and after applying the modal alignment algorithm, where the left hand side shows the initial scrambled modes and the right hand side the aligned modes. It is clear from Fig. 4 that, despite the severe modal inconsistency within each LTI model, Algorithm 1 (Fig. 2) is able to successfully align all the modes sequentially.

The frequency responses have also been generated to examine modal alignment over the entire speed range. Fig. 5 shows the frequency responses of mode #13 before and after the execution of Algorithm 1. It is apparent that the proposed modal alignment algorithm is able to keep track of all the modes successfully over the entire flight profile. It is worth mentioning that $\mathscr{H}_{\sigma-\infty}$ criteria
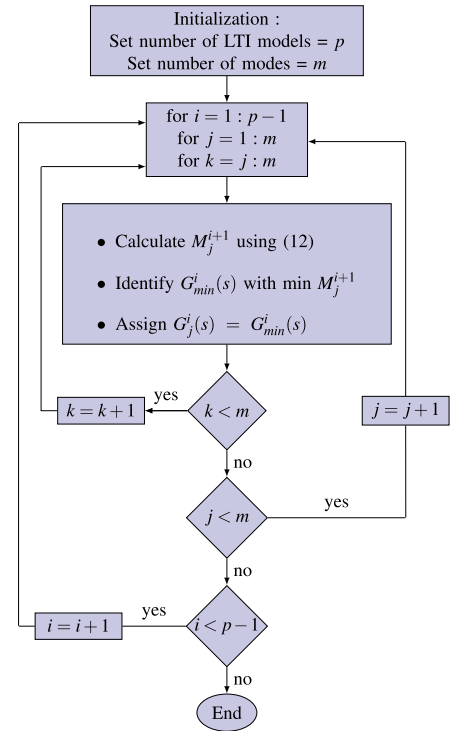

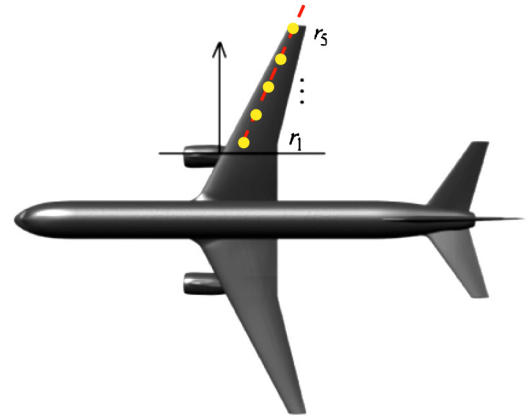**Fig. 2.** Algorithm 1 – modal alignment algorithm.

Fig. 3. GTM with five equally-spaced measurement points along the wing.

have been studied also for mode alignment and produced exactly the same results.[1]

3. Adaptive grid step size determination (AGSSD)

With the current advanced computing power and software capabilities, it is not difficult to generate a large number of LTI models over the gridded parameter space within the flight envelop, for the purpose of improved model accuracy for flight control design. However, from the LPV control design point of view, be it switching [28,29] or non-switching [30], a minimum number of local

---

[1] It is worth mentioning that all flexible modes of the GTM model are complex conjugate. The developed modal alignment algorithm is able to align these modes successfully over the entire range of flight speed. However, other scenarios exist where under-damped complex modes could become over-damped real modes, and vice versa, as flight condition changes. This problem is called "mode veering phenomena". The current mode alignment algorithm is not designed to handle this general scenario nor to handle the defective systems. However, these will be our future research topics.

Table 1
GTM models at various Mach numbers.

Local LTI model	$\mathscr{G}^1$	$\mathscr{G}^2$	$\mathscr{G}^3$	$\mathscr{G}^4$	$\mathscr{G}^5$	$\mathscr{G}^6$	$\mathscr{G}^7$	$\mathscr{G}^8$	$\mathscr{G}^9$	$\mathscr{G}^{10}$	$\mathscr{G}^{11}$	$\mathscr{G}^{12}$	$\mathscr{G}^{13}$	$\mathscr{G}^{14}$	$\mathscr{G}^{15}$	$\mathscr{G}^{16}$	$\mathscr{G}^{17}$	$\mathscr{G}^{18}$
Mach number	0.5	0.52	0.55	0.57	0.60	0.62	0.65	0.67	0.70	0.72	0.74	0.75	0.76	0.77	0.78	0.80	0.85	0.88
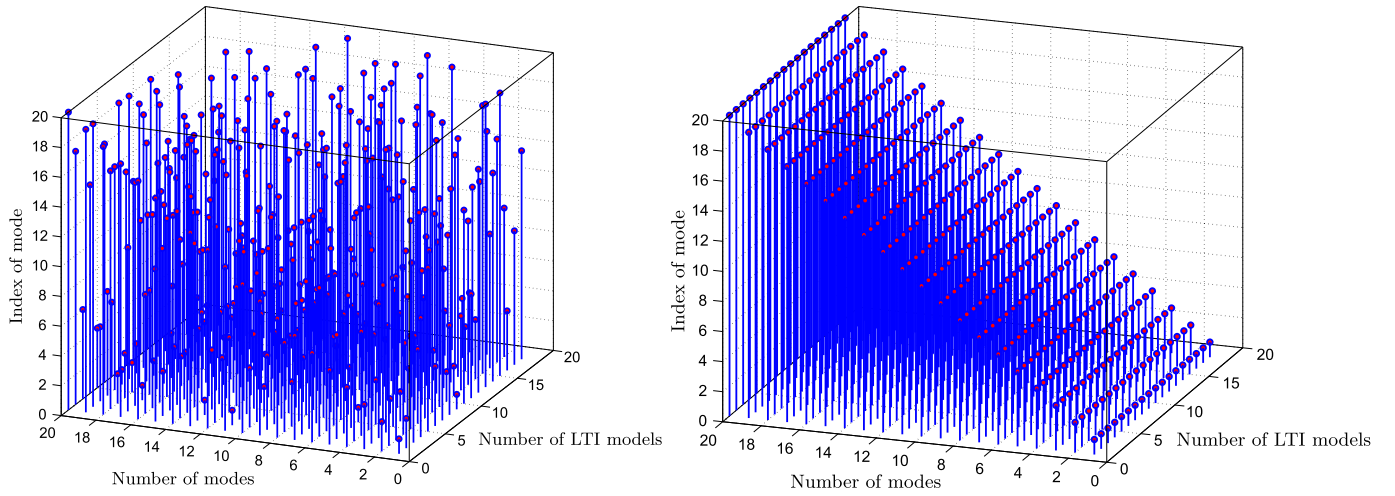
Fig. 4. Modal alignment: scrambled (left) vs. aligned (right).
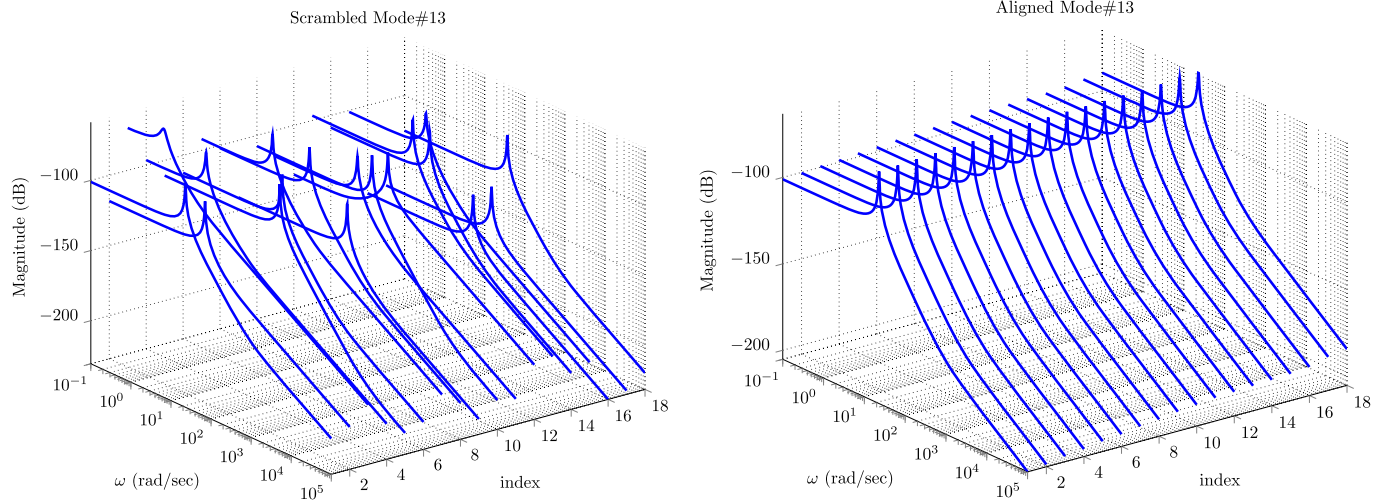
Fig. 5. Frequency response of mode#13: scrambled (left) vs. aligned (right).

LTI models in the problem setup is always desirable, because this would minimize the number of local controllers needed for control design, reduce the number of Linear Matrix Inequalities (LMIs) required for controller synthesis, and eliminate numerical issues during the control design. Now, the challenge is how to reduce the number of LTI models without sacrificing model accuracy. In this section, we propose a novel adaptive algorithm to adjust the grid step size with prescribed error bound. Again, we utilize the notions of $\mathscr{H}_{(\sigma-2)}$- and $\mathscr{H}_{(\sigma-\infty)}$-norm defined earlier as metrics to measure the modeling error.

To this end, we assume all the LTI models in the gridded parameter space have been aligned by following the modal alignment algorithm, Algorithm 1. Let $\|\tilde{\mathscr{G}}^{i,k}(s+\sigma)\|_2$ denote the $\mathscr{H}_{(\sigma-2)}$-norm of the modeling error between $\mathscr{G}^i$ and $\mathscr{G}^{i+k}$, i.e.

$$\|\tilde{\mathscr{G}}^{i,k}(s)\|_{\sigma-2}^2 = \|\mathscr{G}^i(s) - \mathscr{G}^{i+k}(s)\|_{\sigma-2}^2. \tag{13}$$

Let $\delta > 0$ be a prescribed $\mathscr{H}_{(\sigma-2)}$-norm error bound, then all the LTI models between $\mathscr{G}^i$ and $\mathscr{G}^{i+k}$, $k > 1$, can be eliminated, if

$$\|\tilde{\mathscr{G}}^{i,k}(s)\|_{\sigma-2} \leq \delta \quad \text{and} \quad \|\tilde{\mathscr{G}}^{i,k+1}(s)\|_{\sigma-2} > \delta. \tag{14}$$

In other words, if the conditions in (14) are satisfied for a given error bound δ, all the LTI models between indexes i and $i + k$ can be considered redundant and hence eliminated without much impact on the overall model accuracy. The detailed AGSSD process is described in Algorithm 2. Similarly, we can also utilize the $\mathscr{H}_{(\sigma-\infty)}$-norm to compute the modeling error, i.e.

$$\|\tilde{\mathscr{G}}^{i,k}(s)\|_{\sigma-\infty}^2 = \|\mathscr{G}^i(s) - \mathscr{G}^{i+k}(s)\|_{\sigma-\infty}^2, \tag{15}$$

and the same AGSSD algorithm can also be applied to attain the reduced number of LTI models for a given δ error bound. Note that the choice of δ is critical, for it dictates the number of retained LTI models at the end of AGSSD algorithm. To illustrate this, both $\mathscr{H}_{(\sigma-2)}$- and $\mathscr{H}_{(\sigma-\infty)}$-norm are used in AGSSD algorithm to process the 18 LTI aeroelastic GTM models given in Table 1. Fig. 6 shows the number of retained LTI models as functions of $\mathscr{H}_{(\sigma-2)}$ and $\mathscr{H}_{(\sigma-\infty)}$ error bound. As expected, these two norms render different results. However, both norms show that as the requirement on the error bound becomes tighter, additional LTI models

**Algorithm 2.** Adaptive grid step size determination (AGSSD) algorithm.

- Set $\mathscr{H}_{(\sigma-2)}$-norm (or $\mathscr{H}_{\sigma-\infty}$-norm) error bound δ.
- Let $i \leftarrow 1$ and $Ind \leftarrow [1]$; and given $\delta > 0$ and number of LTI models p.

while $i < p - 1$ **do**

    - Let $k \leftarrow 1$.

    while $k \leq p - 1$ **do**

        - Calculate $\|\tilde{\mathscr{G}}^{i,k}(s)\|_{\sigma-2}^2$ using (13) (or $\|\tilde{\mathscr{G}}^{i,k}(s)\|_{\sigma-\infty}^2$ using (15)).

        if $\delta > \|\tilde{\mathscr{G}}^{i,k}(s)\|_{\sigma-2}^2$ (or $\delta > \|\tilde{\mathscr{G}}^{i,k}(s)\|_{\sigma-\infty}^2$) **then**
        | $k \leftarrow k + 1$;
        else if $k = 1$ **then**
        | $Ind \leftarrow [Ind \ \ i+k]$, $i \leftarrow i + k$;
        else
        | $Ind \leftarrow [Ind \ \ i+k-1]$, $i \leftarrow i + k - 1$, $k \leftarrow 1$;
        end
        if $i = p - 1$ **then**
        | $Ind \leftarrow [Ind \ \ i+k]$;
        | **Break**
        else if $i + k > p$ **then**
        | $Ind \leftarrow [Ind \ \ i+k-1]$;
        | **Break**
        end

    end
    if $i + k > p$ **then**
    | **Break**
    end

end

Fig. 6. Number of retained LTI models as function of error bound. *: $\mathscr{H}_{(\sigma-2)}$ norm; $\circ$: $\mathscr{H}_{(\sigma-\infty)}$ norm.

Fig. 7. Time-domain simulations as function of error bound ($\mathscr{G}^6$, Mach 0.62).

will need to be retained in order to meet the prescribed level of model accuracy. For instance, for $\mathscr{H}_{(\sigma-2)}$-norm error bound of 300, we only need to retain eight LTI models out of the original eighteen models to cover the entire flight regime. However, it is still unclear as to what that specific δ error bound means in assessing the level of model mismatch between any two LTI models. To address this, for a given error bound, we need to examine both the time domain and frequency domain responses from the two LTI models and correlate the level of model mismatch to the error bound. Through this exercise, we can determine the acceptable δ error bound and hence the number of retained LTI models in the gridded parameter space to be used for subsequent model reduction. Figs. 7–10 show the time domain and frequency domain comparisons of the linearly interpolated LTI models, $\mathscr{G}^6$ (Mach 0.62) and $\mathscr{G}^{13}$ (Mach 0.76), at two levels of error bound, $\delta = 300$ and $\delta = 600$, based on $\mathscr{H}_{(\sigma-2)}$-norm. As shown, when $\delta = 300$ the responses from interpolated models match very well with those from the exact model, whereas when $\delta = 600$ the responses of the interpolated model shows a large deviation from the actual model.

On the other hand, when utilizing $\mathscr{H}_{\sigma-\infty}$-norm as a metric, at $\delta = 300$ we see that we only need 5 LTI models to cover the entire flight envelop. However, for validation purpose we perform a linear model interpolation between $\mathscr{G}^1$ (Mach 0.5) and $\mathscr{G}^{12}$ (Mach 0.75) to attain the interpolated model $\mathscr{G}^7$ (Mach 0.65). Fig. 11 shows the time-domain simulations of the interpolated $\mathscr{G}^7$ model versus the actual $\mathscr{G}^7$ model, and it shows a large deviation. This indicates that $\mathscr{H}_{\sigma-\infty}$ error bound of 300 is not acceptable, though it renders fewer number of LTI models. Furthermore, if we choose $\mathscr{H}_{\sigma-\infty}$ error bound of 200, we will need 6 LTI models, saving one LTI model compared to the case with $\mathscr{H}_{\sigma-\infty}$ error bound of 300. Fig. 12 shows the validation of the interpolated $\mathscr{G}^5$ (Mach 0.6) derived by interpolating between $\mathscr{G}^1$ (Mach 0.5) and $\mathscr{G}^8$ (Mach 0.67). Similarly, Fig. 13 shows the validation of the interpolated $\mathscr{G}^{10}$ (Mach 0.72) by interpolating $\mathscr{G}^8$ and $\mathscr{G}^{13}$ (Mach 0.76). These time-domain simulations reveal that $\mathscr{H}_{\sigma-\infty}$ error bound of 200 renders an acceptable result.
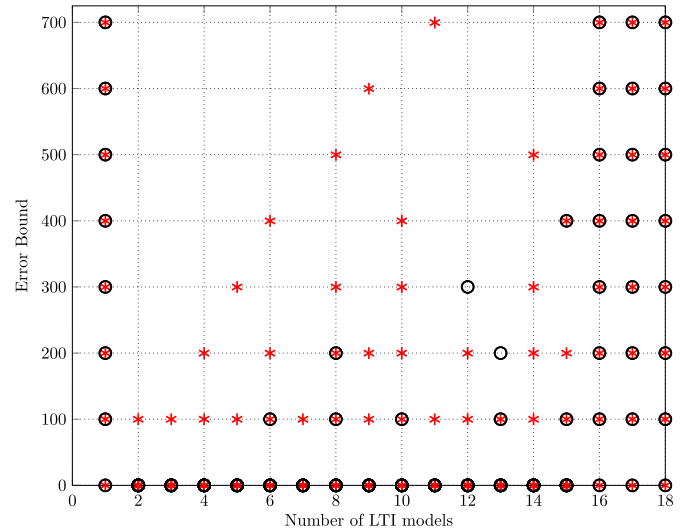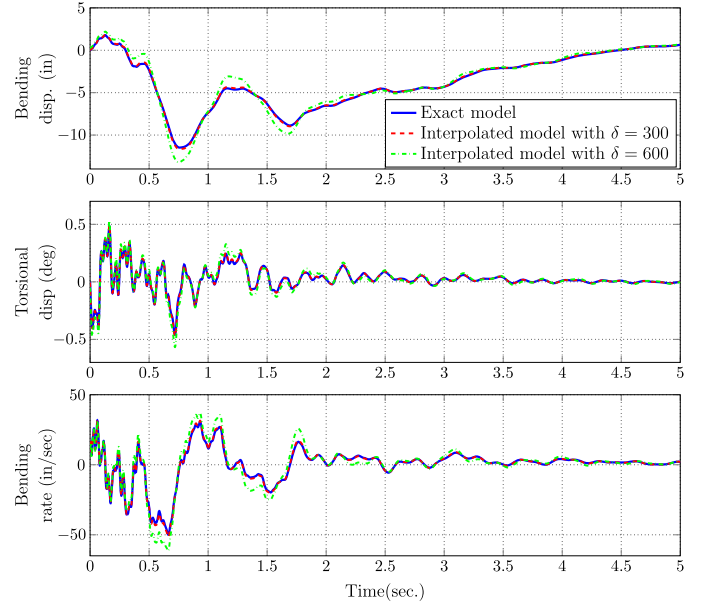
4. Model reduction

Because of the practical limitations on control actuation bandwidth and the needs to lower computational burden in actual implementation, model reduction is often an essential part of modeling and control effort for any physical systems of large dimensions. Following the two algorithms presented in the previous sections, we have attained a reduced number of LTI models with all their modes properly aligned within each LTI model. However, each LTI model still contains very high number of flexible modes. Hence, in this section we introduce the notion of Composite Modal Cost Analysis (CMCA), through which we can attain a reduced-order model that is better suited for flight control design.

4.1. Composite modal cost analysis

The basic idea behind Modal Cost Analysis (MCA) [31,32] is to examine the contribution of each flexible mode to the mission ob-
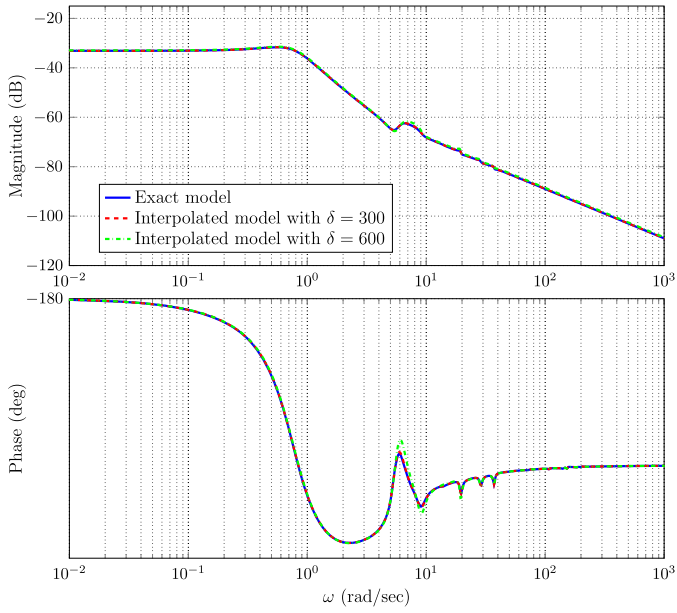
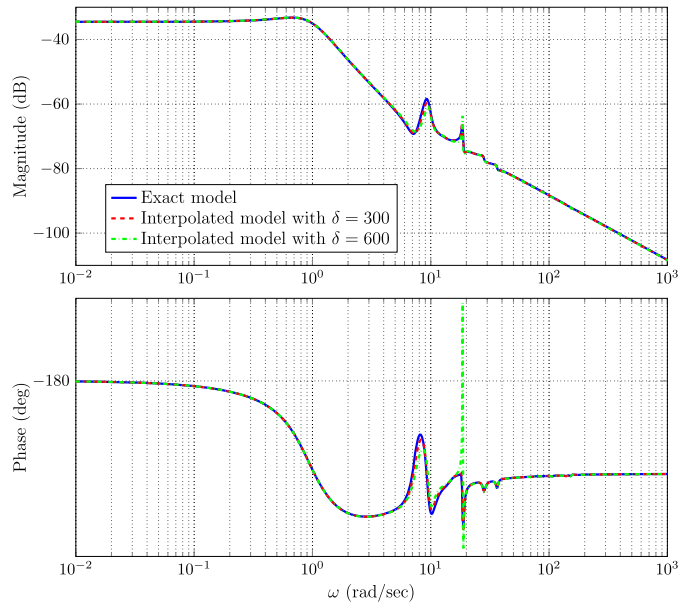**Fig. 8.** Frequency-domain responses as function of error bound ($\mathscr{G}^6$, Mach 0.62).

Fig. 10. Frequency-domain responses as function of error bound ($\mathscr{G}^{13}$, Mach 0.76).
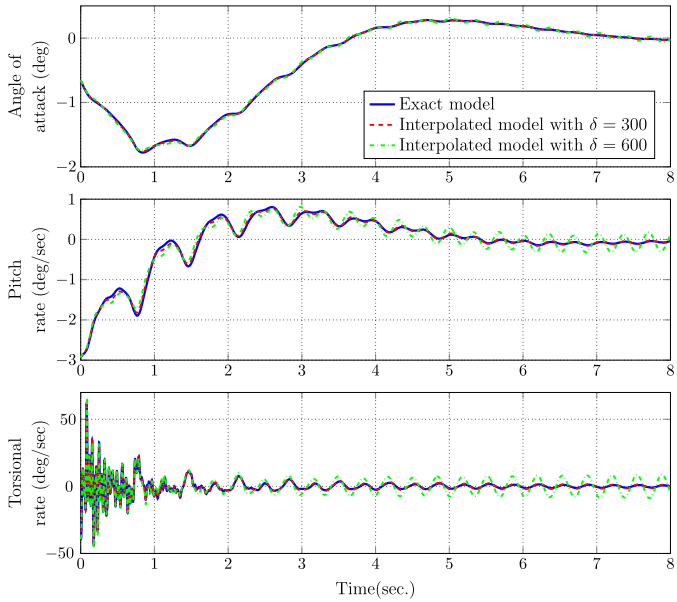

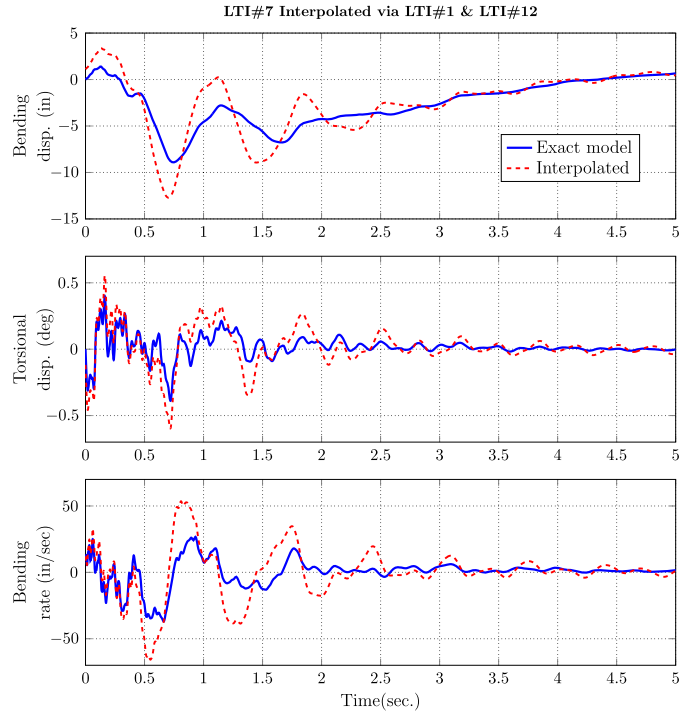**Fig. 9.** Time-domain simulations as function of error bound ($\mathscr{G}^{13}$, Mach 0.76).

Fig. 11. Time-domain simulations of the interpolated $\mathscr{G}^7$ model vs. actual model at $\mathscr{H}_{\sigma-\infty}$ error bound of 300.

jectives in a control system. A metric of modal contribution can be calculated in terms of output covariance, from which contribution of each mode is evaluated and ranked from high to low. This approach is used to derive a reduced-order model from a full-order model by neglecting less significant modes. Recall the modal coordinate representation of a LTI model $\mathscr{G}^i$ described in (2), subjected to the disturbance input,

$$\mathscr{G}^i : \begin{cases} \dot{x}(t) = \mathscr{A}^i x(t) + \mathscr{B}^i u(t) + \mathscr{D}^i w(t) \\ y(t) = \mathscr{C}^i x(t) \end{cases} \quad i = 1, 2, \cdots, p, \quad (16)$$

where $w(t) \in \mathbb{R}^{n_w}$ is the random disturbance input with intensity $W > 0$ and the system matrices $(\mathscr{A}^i, \mathscr{B}^i, \mathscr{C}^i)$ are block matrices as given in (3). Similarly, the matrix $\mathscr{D}^i$ can be partitioned accordingly as follows,

$$\mathscr{D}^i = \begin{bmatrix} D_1^i \\ D_2^i \\ \vdots \\ D_m^i \end{bmatrix}.$$

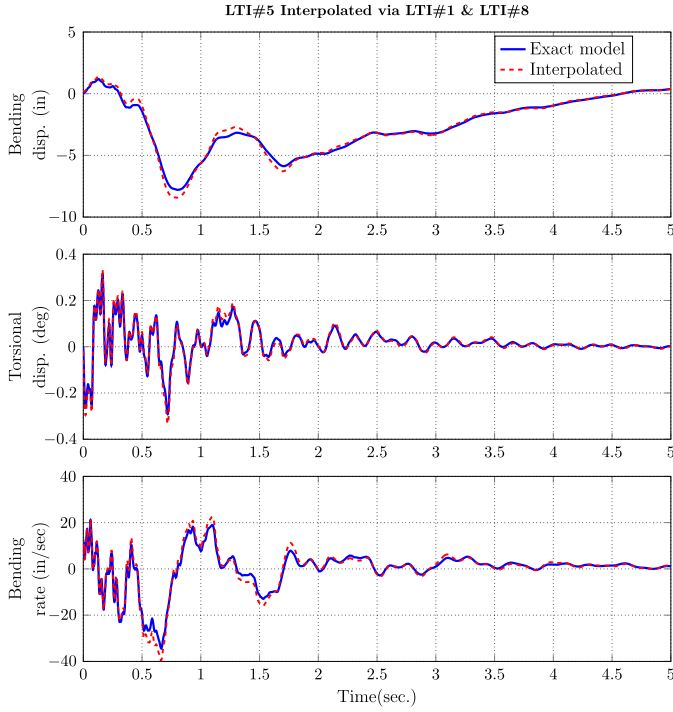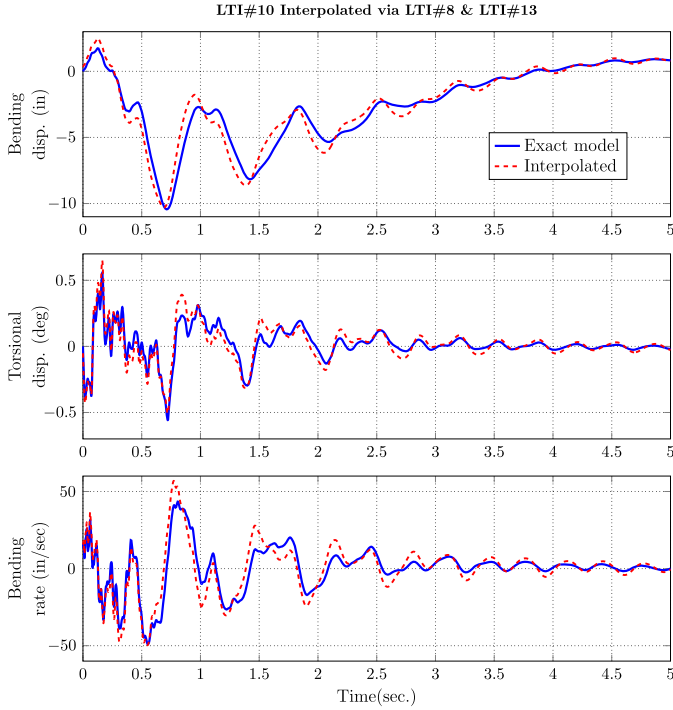If $\mathscr{A}^i$ is Hurwitz, then the open-loop output covariance cost for $\mathscr{G}^i$ is given by [33]

$$Y^i := \text{trace}(\mathscr{C}^i P^i \mathscr{C}^{i'}), \quad i = 1, 2, \cdots, p, \quad (17)$$

where $P^i > 0$ is the controllability Gramian matrix satisfying the following Lyapunov equation,

Fig. 12. Time-domain simulations of the interpolated $\mathscr{G}^5$ model vs. actual model at $\mathscr{H}_{\sigma-\infty}$ error bound of 200.

Fig. 13. Time-domain simulations of the interpolated $\mathscr{G}^{10}$ model vs. actual model at $\mathscr{H}_{\sigma-\infty}$ error bound of 200.

$$P^i \mathscr{A}^{i'} + \mathscr{A}^i P^i + \mathscr{D}^i W \mathscr{D}^{i'} = 0, \quad i = 1, 2, \cdots, p. \quad (18)$$

Let ν_j^i denote the jth modal contribution of ith LTI model $\mathscr{G}^i$ to the output covariance, then noting the modal block partitioning of the matrices $(\mathscr{A}^i, \mathscr{D}^i, \mathscr{C}^i)$, we can deduce that

$$Y^i = \sum_{j=1}^{m} \nu_j^i; \quad \nu_j^i := \text{trace}(C_j^i P^i C_j^{i'}), \quad i = 1, 2, \cdots, p, \quad (19)$$

where $C_j^i P^i C_j^{i'}$ is a 2×2 output covariance matrix corresponding to the jth mode in $\mathscr{G}^i$. This indicates that the total output covariance cost for $\mathscr{G}^i$ can be expressed as a collection of its individual modal contribution. Therefore, we can compute the modal cost of each mode ν_j^i from (19) and rank its contribution from high to low as

$$|\nu_1^i| \geq |\nu_2^i| \geq \cdots \geq |\nu_m^i|, \quad (20)$$

where ν_1^i is the most critical mode and ν_m^i the least critical mode among ν_j^i, $j = 1, \cdots, m$. Note that the modal cost ν_j^i can be a negative value, which indicates that this particular mode is in fact helping to reduce the total cost Y^i, however the total cost is non-negative. Since MCA involves solving the Lyapunov equation (18), it can only be applied to the stable aeroelastic modes for model reduction. Hence, for conventional MCA to work, one must first identify and decompose the modes into stable and unstable modes, and perform MCA only to the stable modes for model reduction. It should be noted that the unstable aeroelastic modes and the aircraft rigid body modes are to be retained by default in the reduced-order model.

To perform the MCA for multiple LTI models covering a wide range of flight regime, we utilize CMCA, in which the collective contribution of each mode is summed up throughout gridded parameter space and its contribution ranked from high to low. In other words, if $\mathscr{M}_j$ denotes the collective contribution of jth mode over all grid points, then its composite modal cost is given by

$$\mathscr{M}_j = \sum_{i=1}^{p} \nu_j^i; \quad \nu_j^i := \text{trace}(C_j^i P^i C_j^{i'}), \quad j = 1, 2, \cdots, m. \quad (21)$$

Similarly, we can compute the composite modal cost for each mode throughout the gridded parameter space and rank its contribution as

$$|\mathscr{M}_1| \geq |\mathscr{M}_2| \geq \cdots \geq |\mathscr{M}_m|, \quad (22)$$

where $\mathscr{M}_1$ is the most contributing mode and $\mathscr{M}_m$ is the least contributing mode among $\mathscr{M}_j$, $j = 1, 2, \cdots, m$. Next, we can utilize the proposed CMCA to each of the 20 aeroelastic modes throughout the 18 LTI models, and the results are given in Table 2. Since there are two unstable modes (1st bending and 1st torsion) at higher flight speeds, they are omitted from CMCA computation, hence only 18 modal costs are shown in Table 2. Fig. 14 shows the modal cost of ν_j^i for $i, j = 1, \cdots, 18$, from which the composite modal cost is derived.

To better handle the cases with unstable modes, we extend the notion of CMCA by introducing a σ-shift transformation to all the modes throughout $\mathscr{G}^i$, $i = 1, \cdots, 18$, so as to "stabilize" all the LTI models in σ-shifted coordinates. Table 3 lists the composite modal cost for all 20 aeroelastic modes after σ-shift, whereas Fig. 15 shows the individual σ-shifted modal cost. Careful examination of Tables 2 and 3 reveals that the most contributing modes are consistent and that the summation of the first four modal costs from Table 2 or first six modal costs from Table 3 amounts to more than 75 % of the total modal cost. Note that the two additional modes italicized in Table 3 are precisely those omitted unstable modes from Table 2. Therefore, we can choose six aeroelastic modes out of 20 modes throughout $\mathscr{G}^i$, $i = 1, \cdots, 18$, to form a reduced-order model suited for control design. Table 4 shows an example of a reduced-order model containing 6 most significant modes at Mach 0.88.

Table 2
Composite modal cost of the stable aeroelastic modes.

Mode index	2	3	6	8	5	7	10	9	18	11	13	17	16	12	15	14	20	19
Total modal cost	468.36	357.93	314.84	161.72	133.46	99.66	82.56	53.19	33.37	28.87	23.10	13.13	11.11	7.28	6.00	3.49	1.36	0.55

Table 3
Composite modal cost of all aeroelastic modes with σ-shift.

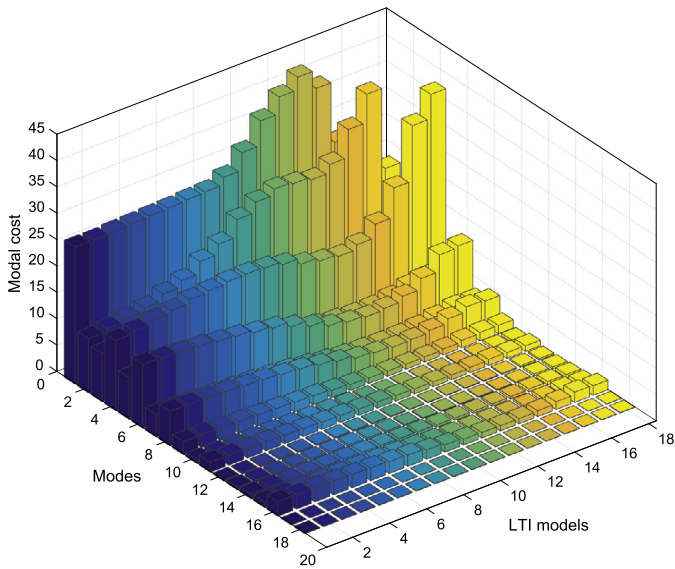| Mode index	2	4	6	3	8	1	7	10	5	18	13	9	11	17	16	12	15	14	20	19
Total modal cost	322.84	299.39	188.44	177.54	158.35	136.86	105.93	104.78	67.30	62.72	38.91	34.45	27.06	24.23	17.73	12.26	8.97	7.56	3.20	1.48

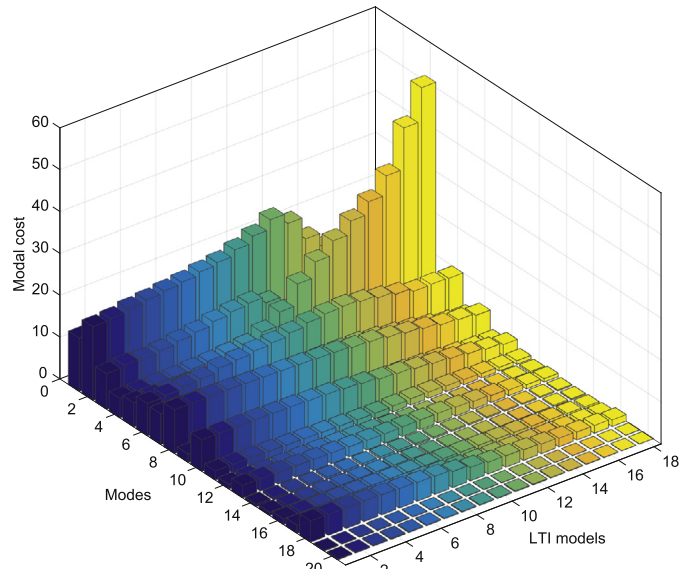Fig. 14. Modal cost of the stable aeroelastic modes.

Fig. 15. Modal costs of all aeroelastic modes after σ-shift.

4.2. Model validation

To validate the proposed model reduction process, we present the root-locus, and the time- and frequency-domain comparisons between the full-order model and the reduced-order model at various flight conditions. For this study, the reduced-order model is consisted of one rigid body short period mode and six aeroelastic modes chosen through the CMCA procedure presented earlier.

Fig. 16 shows the root-locus of the full-order models and reduced-order models over the entire flight envelope. This figure demonstrates the smooth transition of the poles over all grid points, which also verifies alignment of the reduced-order mod-
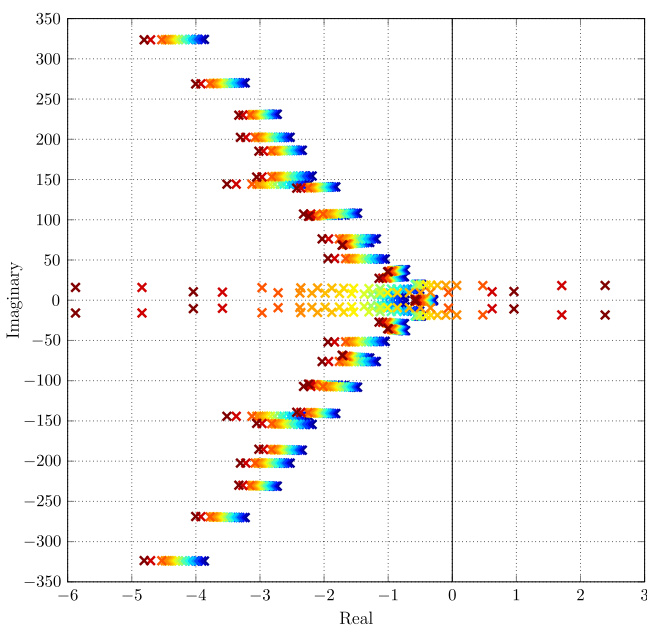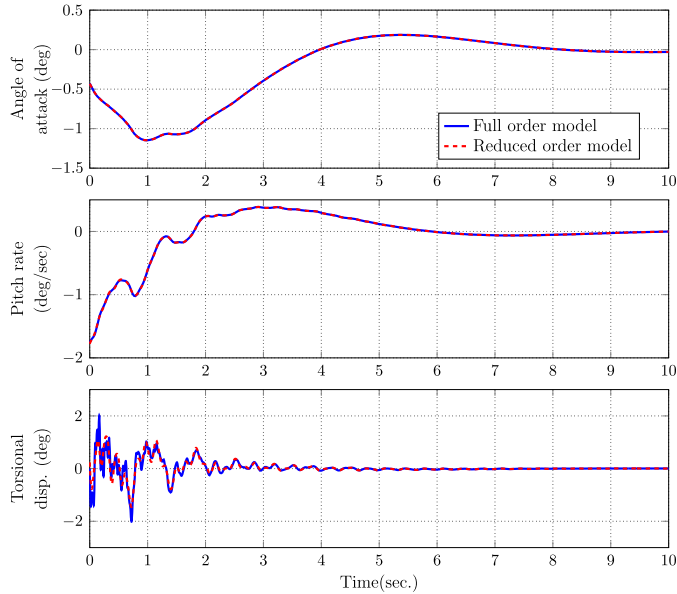

(a) Full-order models.
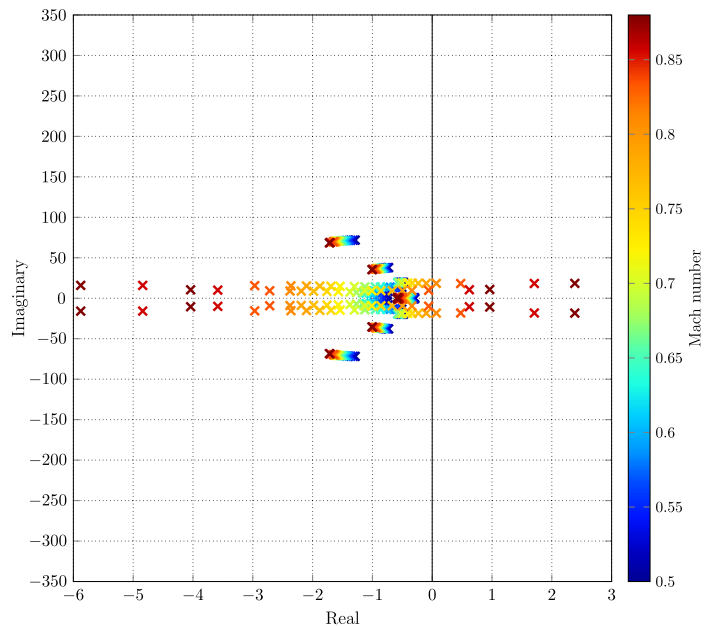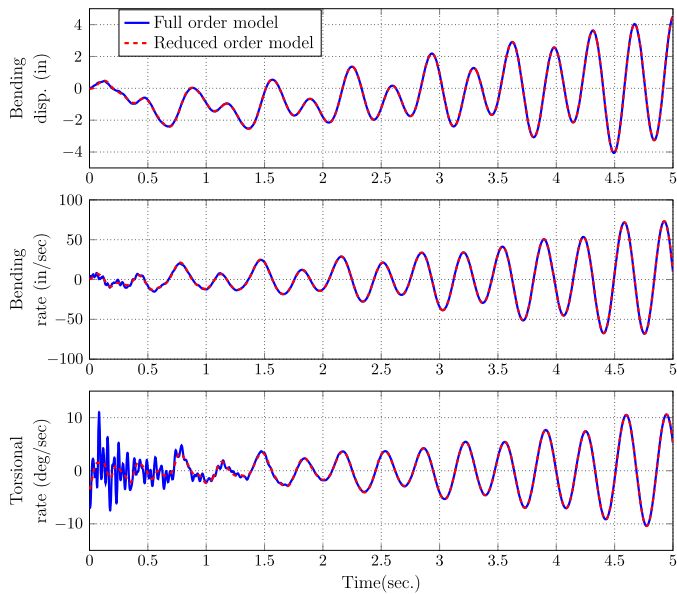

(b) Reduced-order models.

Fig. 16. Root-locus across flight envelope.

Table 4
A reduced-order model with six aeroelastic modes at Mach = 0.88.

| Mode ID	Frequency (rad/sec)	Damping ratio
1st bending (1)	*10.5202*	*−0.0926*
2nd bending (2)	11.27	0.3158
3rd bending (3)	17.0996	0.3451
1st torsion (4)	*18.3889*	*−0.1268*
2nd torsion (6)	35.4116	0.0291
4th bending (8)	68.4175	0.0251

**Fig. 17.** Time-domain simulations at wing tip, Mach = 0.7.

Fig. 18. Time-domain simulations at wing tip, Mach = 0.8.

els. It is clear that the unstable dynamics are kept intact in the reduced-order models and, as expected, the most contributing modes are close to the origin.

Furthermore, a series of time-domain simulations for full- and reduced-order models at Mach 0.7 ($\mathcal{G}^9$) and Mach 0.8 ($\mathcal{G}^{16}$) are conducted, and they are shown in Figs. 17 and 18, respectively. Except at the transient region (for torsional displacement and torsional displacement rate) where high frequency contents dominate,
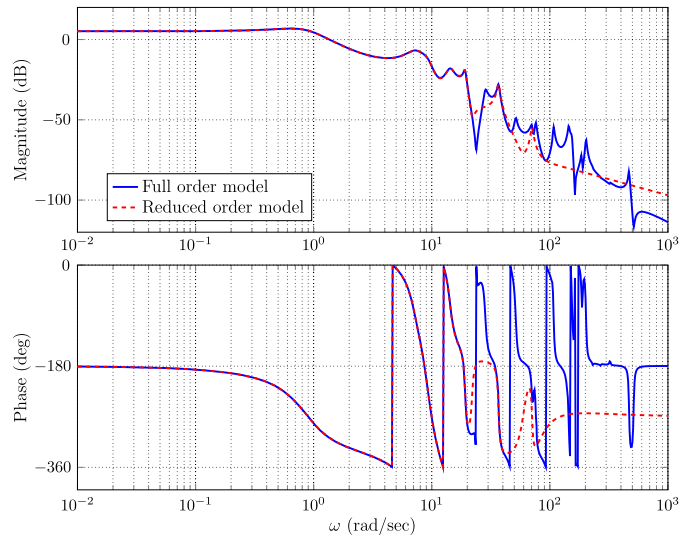
Fig. 19. Frequency responses from disturbance input to bending displacement at wing-tip, Mach = 0.7.
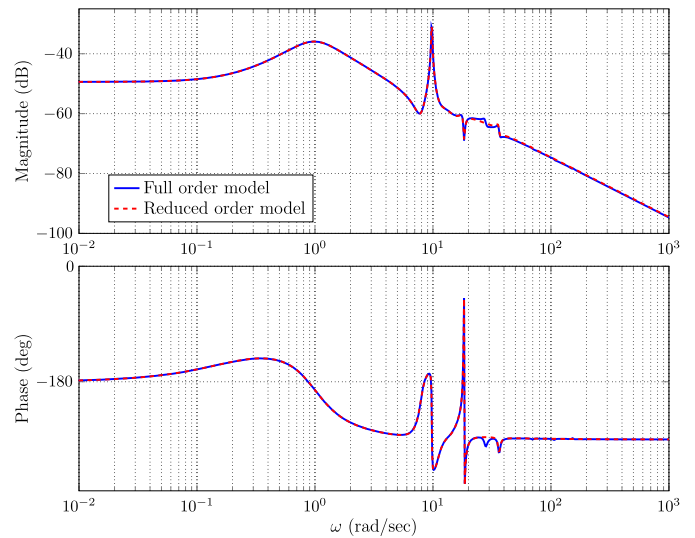
Fig. 20. Frequency responses from disturbance input to pitch rate at wing-tip, Mach = 0.8.

overall the reduced-order model is able to successfully capture both rigid body dynamics and wing-tip aeroelastic behaviors of the full-order model. Similarly, Figs. 19 and 20 show the frequency response comparisons between the full- and reduced-order model at the two flight conditions. The responses are taken from the disturbance input to the wing-tip bending displacement and pitch rate, respectively. These figures show that the reduced-order model is capable of capturing the dynamics of the full-order model at the frequency range of interest.

5. Conclusions

In this paper, we developed a novel modal alignment algorithm to sequentially order the flexible modes for a collection of large dimensional LTI models sampled over the gridded parameter space within the flight envelop. The modal mismatch criteria based on the σ-shifted $\mathcal{H}_2$- and $\mathcal{H}_\infty$-norm were defined and utilized to align modes of similar dynamic behaviors at neighboring LTI models. An Adaptive Grid Step Size Determination algorithm was developed to minimize the number of local LTI models needed to cover the entire gridded parameter space with guaranteed error

bound. This step is especially critical when designing LPV-based flight controllers, in which a problem setup with a small number of local LTI models is highly desirable. Finally, we proposed the concept of composite modal cost analysis and utilized it to attain a reduced-order model that captures essence of the full-order model. Throughout this paper, we used the NASA GTM aeroelastic aircraft models to illustrate the developed algorithms and the model reduction process. The analysis and simulation results demonstrated the effectiveness of the proposed concept.

Conflict of interest statement

There is no conflict of interest.

Acknowledgement

References

[1] J.S. Shamma, M. Athans, Guaranteed properties of gain scheduled control for linear parameter-varying plants, Automatica 27 (3) (1991) 559–564.
[2] W.J. Rugh, J.S. Shamma, Research on gain scheduling, Automatica 36 (10) (2000) 1401–1425.
[3] A. Packard, Gain scheduling via linear fractional transformations, Syst. Control Lett. 22 (2) (1994) 79–92.
[4] P. Apkarian, P. Gahinet, G. Becker, Self-scheduled $\mathscr{H}_\infty$ control of linear parameter-varying systems: a design example, Automatica 31 (9) (1995) 1251–1261.
[5] A.K. Al-Jiboory, G.G. Zhu, J. Choi, Guaranteed performance state-feedback gain-scheduling control with uncertain scheduling parameters, J. Dyn. Syst. Meas. Control 138 (1) (2016) 014502.
[6] J. Mohammadpour, C.W. Scherer, Control of Linear Parameter Varying Systems with Applications, Springer Science & Business Media, 2012.
[7] Y. Hamada, T. Ohtani, T. Kida, T. Nagashio, Synthesis of a linearly interpolated gain scheduling controller for large flexible spacecraft ETS-VIII, Control Eng. Pract. 19 (6) (2011) 611–625, http://dx.doi.org/10.1016/j.conengprac.2011.02.005, http://linkinghub.elsevier.com/retrieve/pii/S0967066111000360.
[8] Z. Prime, B. Cazzolato, C. Doolan, T. Strganac, Linear-parameter-varying control of an improved three-degree-of-freedom aeroelastic model, J. Guid. Control Dyn. 33 (2) (2010) 615–619.
[9] J. Barker, G. Balas, Comparing linear parameter-varying gain-scheduled control techniques for active flutter suppression, J. Guid. Control Dyn. 23 (5) (2000) 948–955.
[10] G. Ferreres, Computation of a flexible aircraft LPV/LFT model using interpolation, IEEE Trans. Control Syst. Technol. 19 (1) (2011) 132–139, http://dx.doi.org/10.1109/TCST.2010.2078510, http://ieeexplore.ieee.org/lpdocs/epic03/wrapper.htm?arnumber=5611633.
[11] R. Tóth, P.S. Heuberger, P.M. Van den Hof, Asymptotically optimal orthonormal basis functions for LPV system identification, Automatica 45 (6) (2009) 1359–1370.
[12] J. De Caigny, R. Pintelon, J.F. Camino, J. Swevers, Interpolated modeling of LPV systems, IEEE Trans. Control Syst. Technol. 22 (6) (2014) 2232–2246, http://dx.doi.org/10.1109/TCST.2014.2300510, http://ieeexplore.ieee.org/lpdocs/epic03/wrapper.htm?arnumber=6731578.
[13] J.-W. van Wingerden, M. Verhaegen, Subspace identification of bilinear and lLPV systems for open- and closed-loop data, Automatica 45 (2) (2009) 372–381.
[14] J. De Caigny, J.F. Camino, J. Swevers, Interpolation-based modeling of MIMO LPV systems, IEEE Trans. Control Syst. Technol. 19 (1) (2011) 46–63, http://dx.doi.org/10.1109/TCST.2010.2078509, http://ieeexplore.ieee.org/lpdocs/epic03/wrapper.htm?arnumber=5620933.
[15] J. Theis, B. Takarics, H. Pfifer, G. Balas, H. Werner, Modal matching for LPV model reduction of aeroservoelastic vehicles, in: AIAA Science and Technology Forum, 2015, pp. 1–12.
[16] C. Poussot-Vassal, C. Roos, Generation of a reduced-order LPV/LFT model from a set of large-scale MIMO LTI flexible aircraft models, Control Eng. Pract. 20 (9) (2012) 919–930, http://dx.doi.org/10.1016/j.conengprac.2012.06.001, http://linkinghub.elsevier.com/retrieve/pii/S0967066112001220.
[17] B. Takarics, P. Baranyi, Tensor-product-model-based control of a three degrees-of-freedom aeroelastic model, J. Guid. Control Dyn. 36 (5) (2013) 1527–1533, http://dx.doi.org/10.2514/1.57776, http://arc.aiaa.org/doi/abs/10.2514/1.57776.
[18] P. Baranyi, B. Takarics, Aeroelastic wing section control via relaxed tensor product model transformation framework, J. Guid. Control Dyn. 37 (5) (2014) 1671–1677.
[19] H. Hughes, F. Wu, $\mathscr{H}_\infty$ LPV state feedback control for flexible hypersonic vehicle longitudinal dynamics, in: AIAA Guidance, Navigation, and Control Conference, AIAA, Toronto, Canada, 2010, pp. 1–13.
[20] D.H. Baldelli, R. Lind, M. Brenner, Robust match-point solutions using describing function method, J. Aircr. 42 (6) (2005) 1596–1604.
[21] S. Bennani, J.-W.V. Staveren, B. Beuker, J.J. Meijer, Flutter analysis of an f-16a/b in heavy store configuration, J. Aircr. 42 (6) (2005) 1565–1574.
[22] A. Varga, A. Hansson, G. Puyou, Optimization based clearance of flight control laws, in: Lecture Notes in Control and Information Science, Springer, 2012, pp. 11–36.
[23] G. Puyou, Y. Losser, Clearance benchmark for a civil aircraft, in: Optimization Based Clearance of Flight Control Laws, Springer, 2012, p. 121.
[24] C. Roos, Generation of flexible aircraft LFT models for robustness analysis, 6th IFAC Symposium on Robust Control Design 42 (6) (2009) 349–354, http://dx.doi.org/10.3182/20090616-3-IL-2002.00060, http://www.sciencedirect.com/science/article/pii/S1474667015404276.
[25] C.P.M. Chicunque, Linear, Parameter-Varying Control of Aeroservoelastic Systems, Ph.D. thesis, University of Minnesota, 2015, http://conservancy.umn.edu/handle/11299/175269.
[26] S.S. Rao, Mechanical Vibrations, Prentice Hall, 2011.
[27] G. Zhu, M. Rotea, R. Skelton, A convergent algorithm for the output covariance constraint control problem, SIAM J. Control Optim. 35 (1) (1997) 341–361.
[28] M. Hanifzadegan, R. Nagamune, Smooth switching LPV controller design for LPV systems, Automatica 50 (5) (2014) 1481–1488.
[29] B. Lu, F. Wu, Switching LPV control designs using multiple parameter-dependent Lyapunov functions, Automatica 40 (11) (2004) 1973–1980, http://dx.doi.org/10.1016/j.automatica.2004.06.011, http://linkinghub.elsevier.com/retrieve/pii/S0005109804001840.
[30] P. Apkarian, R.J. Adams, Advanced gain-scheduling techniques for uncertain systems, IEEE Trans. Control Syst. Technol. 6 (1) (1998) 21–32, http://ieeexplore.ieee.org/xpls/abs_all.jsp?arnumber=654874.
[31] R.E. Skelton, P.C. Hughes, H. Hablani, Order reduction for models of space structures using modal cost analysis, J. Guid. Control Dyn. 5 (4) (1982) 351–357.
[32] S.S. Swei, G.G. Zhu, N.T. Nguyen, Integrated model reduction and control of aircraft with flexible wings, in: AIAA Guidance, Navigation, and Control Conference, http://dx.doi.org/10.2514/6.2013-4862.
[33] R.E. Skelton, Dynamic Systems Control: Linear Systems Analysis and Synthesis, John Wiley & Sons, 1988.